

Optimization of a Heat Pipe Microreactor Heat Exchanger for a Supercritical Carbon Dioxide Brayton Cycle

Mitchell R Erickson*, Curtis H. Foster[†], Gregory F. Nellis[‡], Mark H. Anderson

*Department of Mechanical Engineering, University of Wisconsin-Madison
1500 Engineering Dr, Room *1337, [†]1337, [‡]1339, 1305 Madison, WI 53706
merrickson4@wisc.edu, chfoster2@wisc.edu, gfnellis@engr.wisc.edu, manderson@engr.wisc.edu*

Abstract.

Microreactors are small, micro-modular nuclear reactors that effectively provide clean power to any remote, decentralized application. They can be embedded with heat pipes that utilize the phase change of liquid metal to efficiently transport thermal energy from the reactor core to the end-user application with minimal moving parts. The heat pipe integration heat exchanger couples the nuclear reactor with a working fluid of a power block and is critical to reliability and performance. Optimization of a printed circuit heat exchanger microchannel was performed to maximize performance and efficiency using computational fluid dynamics simulations and supercritical carbon dioxide (sCO₂) Brayton cycle analyses. A comparison to recuperated air Brayton cycles was performed and found the sCO₂ cycle to have significantly increased efficiencies. Finally, a comparison to an annular flow heat exchanger was conducted and found a heat exchanger performance insensitivity to sCO₂ cycle efficiency.

1. Introduction

Microreactors have recently been considered as an effective energy source for applications where other methods are uneconomical or unavailable. Microreactors are factory manufacturable, easily transportable, produce <50 MW_e of energy, and maintain a neutronic simplicity to allow autonomous operation [1]. They are an effective method to provide clean power to desalination, hydrogen production, chilled water production, and any remote application, including disaster relief, military installations, and remote communities. The U.S. Department of Energy has created the Microreactor Program to advance technological readiness of microreactors and their applications [2]. The objectives of this program are to assist existing developers in meeting their interdisciplinary R&D needs; develop a framework to support design, development, experimentation, and model validation; and improve microreactor performance, economics, and integration. This program has prioritized technological maturation of microreactor heat removal technology and creating coupling components for power conversion applications.

A heat pipe microreactor utilizes high-temperature heat pipes to efficiently transport thermal energy from the monolithic reactor core to the end-user application. This approach minimizes moving parts and is robust and fault tolerant. The heat pipe micro-reactor has been considered for space power applications and is currently being considered for any remote application requiring safe, reliable, affordable, and transportable power. The heat pipes are filled with liquid metal and boast a thermal conductivity much higher than that of any metal while passively circulating through the evaporation and condensation of the working fluid. The microreactor applies heat to the evaporator, causing vapor to flow down the heat pipe. An end-user application removes heat from the condenser and the liquid is returned through capillary action in a wick.

An example of a heat pipe microreactor being developed is Westinghouse's eVinci Microreactor [3]. This is a micro-modular reactor that can produce 5 MW_e with 15 MW_{th} (Figure 1). It is an easily transportable solution that provides rapid deployment to decentralized remote applications without the need of water for cooling and operation. This microreactor is designed to be passively safe, utilizing heat pipes, TRISO fuel, and a passive heat removal system.



Figure 1. Westinghouse's eVinci reactor [4]

A significant challenge with any microreactor application is the integration of the reactor itself with the end-user application. The heat pipe integration heat exchanger is a high-cost component of the microreactor system that is critical to its overall reliability and performance. Significant research initiatives have focused on the microreactor core and the overall system, however, there is a need to research the primary heat exchanger required to interface the heat pipe condenser with the process fluid of a power cycle.

Guillen and McDaniel [4] evaluated different power conversion cycles for land-based nuclear microreactor applications. They analyzed steam, air Brayton, sCO₂ Brayton, and Stirling cycles based upon technical maturity, system efficiency, size, cost, safety, and siting considerations. From this, they recommended the recuperated air Brayton cycle be further researched for microreactor applications, though, they noted the uncertainty in sCO₂ estimates. They suggest future development of compact, highly efficient heat exchangers to transfer heat from heat pipes to the working fluid. Because of this, initial advancements in microreactor technology have been focused on air Brayton systems.

Alternatively, other researchers have suggested using sCO₂ cycles for microreactor applications because of their high efficiency and smaller turbomachinery [5][6]. Previous work has focused on the design, optimization, and experimentation of a primary heat exchanger with air as the working fluid. This paper focuses on the design and optimization of a microreactor heat pipe interfaced heat exchanger for an sCO₂ cycle.

The primary heat exchanger designs considered are the annular flow heat exchanger (AFHX) and printed circuit heat exchanger (PCHE). Previously, an evaluation of the AFHX has been completed for heat pipe microreactor applications [7]. This design forces fluid axially along the heat pipe, flowing within an annulus and removing heat. This design is shown in Figure 2. The PCHE design is a plate-fin type heat exchanger. Microchannels are chemically etched into thin plates, defining the flow path. These plates are stacked together and diffusion bonded, creating a highly efficient heat exchanger. These heat exchangers have high heat transfer coefficients, high heat transfer area, and can withstand high operating pressures. The bonded plates are placed over the heat pipes, causing the fluid to flow in a crossflow manner, shown in Figure 3. This ensures that heat is consistently drawn from the heat pipe, unlike the AFHX which changes heat transfer rate and temperature axially. Finally, PCHEs boast a high effectiveness and low pressure drop, creating higher cycle efficiencies.

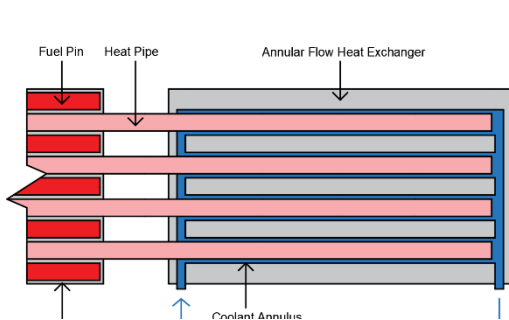


Figure 2. Annular flow heat exchanger [7]

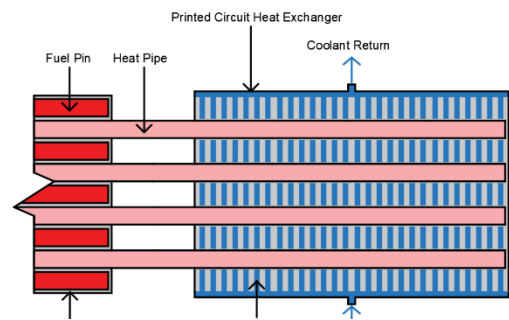


Figure 3. Printed circuit heat exchanger [7]

Previously, AFHXs and PCHEs were analyzed to integrate a 5 MW_{th} heat pipe microreactor to a recuperated air Brayton power cycle [8]. Optimization of the AFHX annulus and PCHE microchannel was performed, and it was found that cycle efficiencies were highly dependent on pressure losses through the heat exchanger. This pressure limitation constrained the heat exchanger designs to larger hydraulic diameters. This constraint is removed with the sCO₂ cycle's higher operating pressure, allowing for more detailed optimization of the microchannel geometry. The work presented will introduce the cycle model used to analyze the heat exchangers, explain the methodologies used to create accurate PCHE predictions, and report results obtained from this optimization analysis.

2. System Model

The system model analyzes a sCO₂ recompression Brayton cycle coupled to a 5 MW_{th} reactor. The main components in the cycle are the main compressor, recompression compressor, low temperature recuperator (LTR), high temperature recuperator (HTR), primary heat exchanger, turbine, and air cooler, shown in Figure 4. The sCO₂ is split after the hot-side LTR, forcing the smaller stream to bypass the air chiller. These streams reconvene after the cold-side LTR where they are heated in the HTR and primary heat exchanger. Finally, the sCO₂ is expanded in the turbine, spinning a shaft to generate electricity. The assumptions of each cycle component are listed in Table 1.

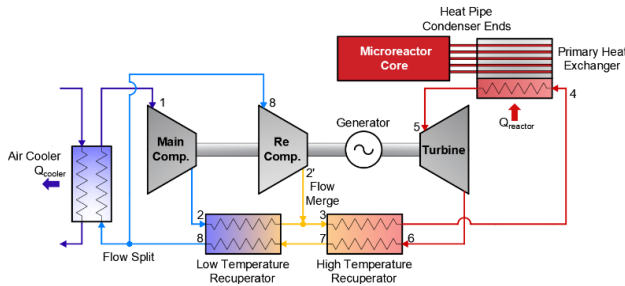


Table 1. Cycle component assumptions

Main/Re. compressor isentropic efficiency	90%
HTR/LTR effectiveness	95%
HTR/LTR power losses	1%
Turbine isentropic efficiency	90%
Air cooler fan efficiency	41%

Figure 2. sCO₂ recompression Brayton cycle schematic [7]

This model assumes a constant 5 MW_{th} of heat input into the evaporator end of the heat pipe. A schematic of a sodium filled heat pipe is shown in Figure 5. It is comprised of a wall, liquid annulus, capillary wick, and vapor core. Heat is added to the evaporator section of the heat pipe, vaporizing the liquid metal. This creates a pressure gradient axially, forcing vapor to flow towards the condenser. Heat is removed at the condenser, condensing the liquid and pumping it back through the wick via capillary action, restarting the cycle. A series of resistances are used to model the temperature drop through the heat pipe, including resistance through the evaporator pipe wall, evaporator wick, vapor passage, condenser wick, and condenser pipe wall [9]. This process defines the temperature at the interface of the heat exchanger.

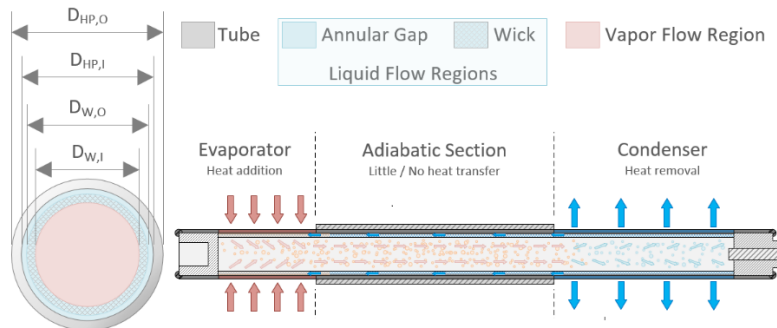


Figure 3. Heat pipe operation diagram

The reactor design used in this analysis is the Special Purpose Reactor developed by Los Alamos National Lab [10]. This heat pipe reactor outputs 5 MW_{th} using low-enriched uranium oxide fuel. It has a hexagonal, stainless steel monolithic core containing 2112 fuel pins and 1224 liquid metal potassium heat pipes.

The air cooler model was developed by Pidaparti to verify performance of commercially available air coolers [11]. The model returns the fan power requirements and working fluid pressure drop for various cycle parameters, specifically the inlet state, outlet pressure, and mass flow rate. Results were calculated for two air cooler heat exchangers with a fan efficiency of 41% and 30° C ambient air. Using these fan inputs, a low pressure of 7.7 MPa, and a pressure ratio of 2.65, the optimal recompression fraction was found to be 0.375.

3. CFD Optimization

Optimization of the internal geometry of the sCO₂ PCHE was done to increase the heat transfer performance by facilitating fluid movement towards the walls of the heat pipes. The objectives of this optimization were to increase heat transfer and minimize pressure drop to maximize cycle efficiency. The air Brayton cycle was sensitive to pressure losses in the primary heat exchanger, forcing the exclusion of inner-microchannel geometries. Since sCO₂ operates at high cycle pressures and is denser fluid, enhanced optimization was performed. The metrics of importance are the approach temperature difference and the pressure drop of the unit cell.

$$\Delta T_{approach} = T_{HP,max} - T_{out} \quad (1)$$

$$\Delta P_{CFD} = P_{out} - P_{in} \quad (2)$$

Conjugate heat transfer simulations were conducted in ANSYS Fluent. The steady state SIMPLE method was used with RANS $k - \omega$ models employed. The baseline geometry unit cell to be optimized is shown in Figure 6. This unit cell is a single plate of the PCHE and represents the last five rows of a 1/12th wedge of the entire heat exchanger. The sCO₂ fluid is shown in blue and the 316SS is shown in gray. The flow enters the unit cell on the right and exits to the left. The unit cell inlet temperature was calculated from an energy balance to be 621° C, the inlet pressure was set to be 20 MPa, and the mass flow rate was set to be 24 kg/s throughout the entire 0.8 m tall PCHE with 533 microchannels. A symmetric boundary condition was applied on the top edge, centerline, and front face. A pressure inlet and mass flow outlet were used as shown in black.

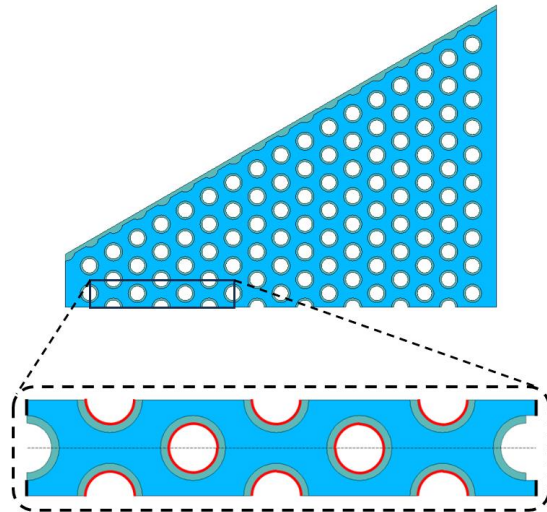


Figure 4. (top) 1/12th wedge of PCHE, (bottom) baseline CFD unit cell of PCHE

Thermal boundary conditions, equivalent to 5 MW, were applied on the heat pipe walls, shown in red. Heat pipes operate at a constant temperature because of the phase change at the condenser but output a constant average heat flux. Because of this, neither a constant temperature nor constant heat flux boundary condition is representative of the true boundary. Thus, a heat flux-derived temperature boundary condition was created to simulate this phenomenon, shown below.

```

for time-step
  for zone in zones
    if zone == thermalBoundaryCondition
       $T_{bc,new} = T_{bc,current} + \alpha_p(HF_{req} - HF_{current})$ 
    end
  end
end
end

```

This function uses a PI controller to vary the temperature boundary condition until the correct average heat flux is achieved.

Initial low-fidelity simulations were done on many channel geometries (Figure 7). The best performing geometry was the containment which directed flow towards the heat pipe walls, increasing velocity and heat transfer coefficients. This geometry was chosen for further refinement.

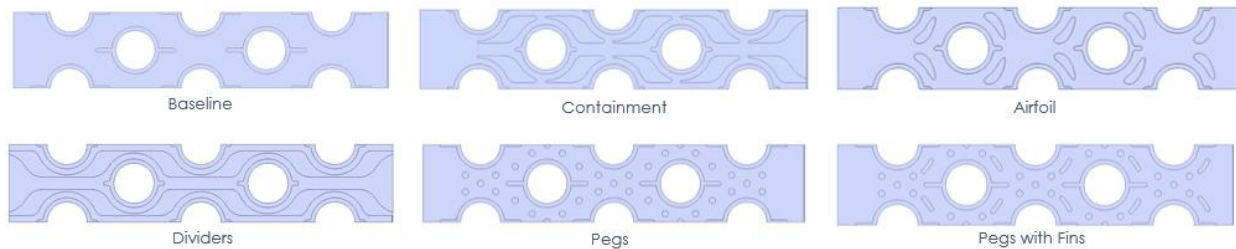


Figure 5. Initial geometry analysis

To obtain reliable results, a mesh sensitivity analysis was performed on the containment geometry. Sufficient mesh insensitivity was achieved in temperature and pressure for higher fidelity meshes. For all remaining CFD results, approximately $O(10^6)$ cells were used.

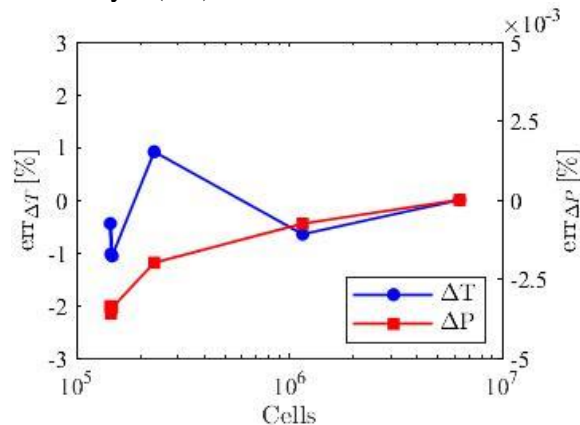


Figure 6. Mesh sensitivity results

The gap thickness of the containment geometry, shown in Figure 9, was optimized. This thickness varied between 0.25 – 1.5 mm. The chemical etching depth was set to be half of this gap thickness, per a manufacturing constraint. Separations in the flow paths are included in the geometry to allow cross flow in the case of channel blockages. Pockets of increased hydraulic diameter were added between heat pipes to minimize friction losses. The temperature and velocity magnitude contours are shown in Figure 9 for the

baseline and containment geometries on the left and right, respectively. Looking at the baseline temperature and velocity contours, there is a hotspot and stagnation zone behind the heat pipe wall. These effects are minimized in the containment geometry because of the inner-channel walls forcing the fluid towards the heat pipe wall. The results of the gap thickness optimization are shown in Figure 10 where approach temperature difference is plotted against the pressure drop of the unit cell. The gap thickness is decreasing from left to right.

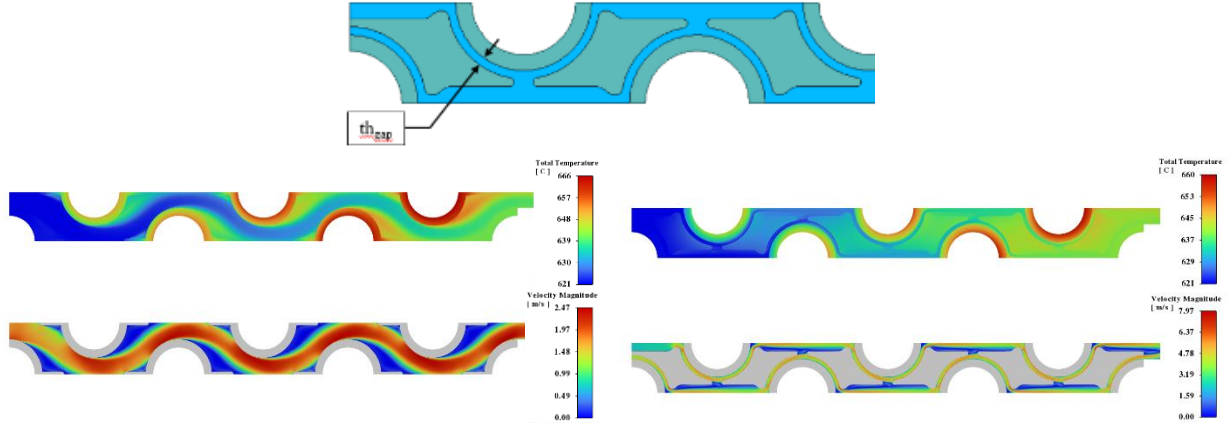


Figure 7. (top) Containment geometry, (middle) temperature contours, (bottom) velocity contours, (left) baseline results, (right) containment results

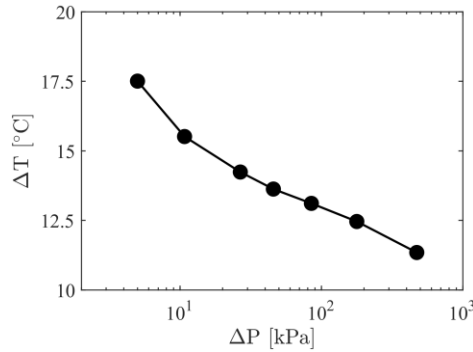


Figure 8. Approach temperature difference vs pressure drop of the unit cell for varying gap thicknesses

To extrapolate these results to the entire heat exchanger, the approach temperature difference found from the CFD simulations were the same as the heat exchanger ($\Delta T_{PCHE} = \Delta T_{CFD}$). This approach temperature difference was assumed to be constant and independent of mass-flow rate and inlet temperature. These assumptions are valid as the cycle mass flow rate and heat exchanger inlet temperature are close to 24 kg/s and 490° C. The pressure drop throughout the PCHE was calculated using a modified Bernoulli's equation that utilized a loss coefficient, k , that captures major and minor losses. This equation is shown below:

$$P_{in} + \frac{\rho_{in} V_{in}^2}{2} = P_{out} + \frac{\rho_{out} V_{out}^2}{2} + k \frac{\rho_m V_m^2}{2} \quad (3)$$

where P is pressure, V is velocity, and ρ is density, calculated at the inlet, outlet, and middle locations. The loss coefficient was calculated using the CFD simulation results.

A 1/12th wedge of the PCHE was discretized into rows of heat pipes to be modeled in the sCO₂ cycle (Figure 11). An energy balance was performed on a single row of heat pipes, which resulted in a row-outlet temperature. Equation 3 was performed on a single row to calculate row-outlet pressure. The middle values in Equation 3 were taken as linear interpolations of the row-inlet and -outlet values. Velocities were calculated using densities, the cycle mass flow rate, and cross-sectional areas. This process was solved implicitly in the software Engineering Equation Solver and resulted in PCHE pressure drop. The results of this process are shown in Figure 12.

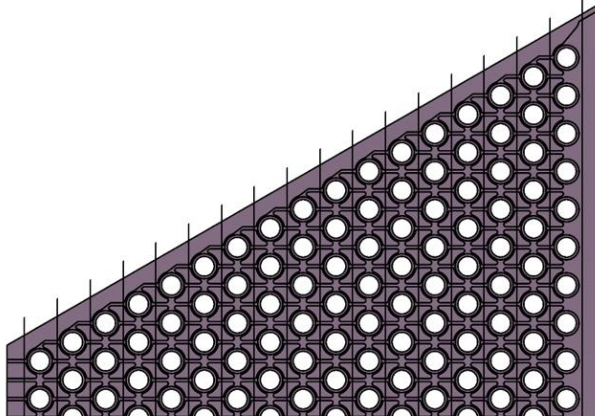


Figure 9. Discretized 1/12th wedge

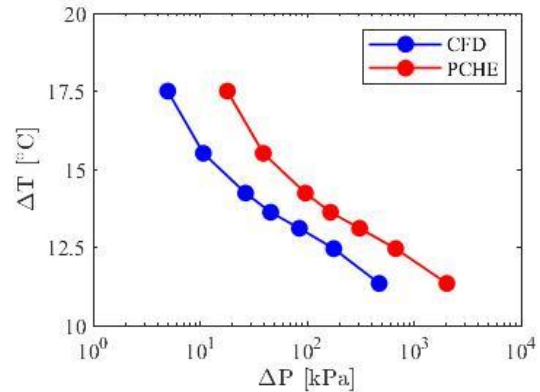


Figure 10. Approach temperature difference vs pressure drop for CFD and PCHE results

4. Results

The cycle efficiency versus gap thickness relationship is shown in Figure 13, where the optimal gap thickness is 1.25 mm. Optimization from the baseline to the 1.25 mm containment geometry resulted in a 38% decrease in approach temperature difference and an 870% increase in pressure drop, though this pressure drop within the PCHE represents 0.05% of the total pressure drop within the cycle. Table 2 shows the performance and cycle efficiencies of the AFHX and PCHE within a recuperated air Brayton and recuperated sCO₂ cycle model.

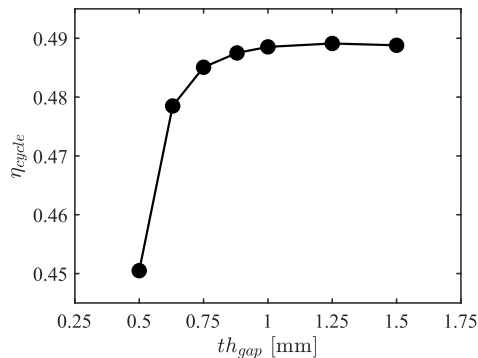


Figure 11. Cycle efficiency vs gap thickness

Table 2. Performance and cycle efficiencies for AFHX and PCHE

Heat Exchanger	Annular/PCHE Gap	Cycle Efficiency	ΔP [kPa]	ΔT [°C]
AFHX (air) [8]	1.9 mm	34.3 %	32.6	51.1
PCHE (air) [8]	1.0 mm	36.4 %	14.2	43.1
AFHX (sCO ₂)	0.9 mm	48.9 %	8.5	4.1
PCHE (sCO ₂)	1.25 mm	48.6 %	39.0	15.5

The sCO₂ Brayton cycle shows a significant improvement in cycle efficiency for both heat exchangers when compared to the air Brayton cycle. The sCO₂ Brayton cycle efficiency calculated is similar to the value reported by Guillen and McDaniel of 48%. The air Brayton cycle efficiency falls short of their predicted efficiency of 43%. This can be explained by the air Brayton cycle's sensitivity to pressure drop through the heat exchanger, caused by the lower density of air and the lower operating pressure of the cycle.

This constrains the heat exchanger design and thus limits the performance. $s\text{CO}_2$, however, operates at higher pressures and has a higher density, allowing for the construction of microchannel designs to maximize the heat exchanger performance.

The AFHX performs better than the PCHE with lower pressure drop and approach temperature difference. However, the AFHX provides only a 0.3% efficiency increase, showing that the cycle is less sensitive to heat exchanger performance. PCHEs are technologically mature and are capable of handling the pressures required of a $s\text{CO}_2$ cycle. On the contrary, the manufacturing maturity of AFHXs are not ready, limiting their feasibility in this application. For example, techniques to seal the high pressure boundary of the heat pipe ends must be researched. Furthermore, the axial temperature gradients in an AFHX may limit the performance of the heat pipe that requires specific temperatures to operate efficiently.

5. Conclusion and Future Work

RANS CFD simulations were used to analyze and optimize microchannel geometries of a PCHE. Approach temperature difference and pressure drop results were extrapolated to predict the performance of the entire heat exchanger using a modified Bernoulli's equation. The PCHE was analyzed in an $s\text{CO}_2$ cycle model, finding the optimal gap thickness to be 1.25 mm. This design resulted in improved thermal performance over the baseline design. The $s\text{CO}_2$ results showed a significant efficiency increase over the air Brayton cycle.

The optimized $s\text{CO}_2$ PCHE has been designed and sent out for manufacturing. Experimental testing will be performed to demonstrate heat exchanger performance and model validity. Investigation into the manufacturing methods of both PCHE and AFHX technologies will be completed. Moreover, leveled cost of electricity analyses and investigations into heat exchanger headerings will be conducted.

Acknowledgements

This work was funded in part by the University of Wisconsin under the Faustin Prinz Fellowship Program, along with the Department of Energy Office of Nuclear Energy's Nuclear Energy University Program under Award Number DE-NE0009141. The views and opinions of authors expressed herein do not necessarily state or reflect those of the United States Government or any agency thereof.

References

- [1] Kennedy, J. C., et al., “Special Purpose Application Reactors: Systems Integration Decision Support,” INL/EXT-18-51369-Rev001, INL, (2019).
- [2] Jackson, J. H., and Sabharwall, P., “Foreword: Special issue on the U.S. Department of Energy Microreactor Program,” *Nuclear Technology*, 209:sup1, iii-v, (2023).
- [3] Westinghouse, “Energy Systems,” <https://www.westinghousenuclear.com/energy-systems/evinci-microreactor> (accessed Dec. 12, 2024).
- [4] Guillen, D. P. and McDaniel, P. J., “An evaluation of Power Conversion Systems for land-based nuclear microreactors: Can aeroderivative engines facilitate near-term deployment?,” *Nuclear Engineering and Technology*, vol. 54, no. 4, pp. 1482–1494, (2021).
- [5] Sabharwall, P., Kim, E. S., McKellar, M., and Anderson, N., “Process Heat Exchanger Options for the Advanced High Temperature Reactor,” INL/EXT-11-21584, INL, (2011).
- [6] Trellue, H. R., et al., “Microreactor Demonstration and Testing Progress in FY19,” LA-UR-19-28768, LANL, (2019).
- [7] Foster, C., Erickson, M., Nellis, G., Anderson, M., “Optimal Microreactor Heat Pipe Heat Exchanger Microchannel Design for a Supercritical CO₂ Brayton Cycle”, *ANS Annual Winter Conference and Expo*, Orlando, FL, (2024).
- [8] Foster, C., et al., “Impacts of Heat Exchanger Design on Heat Pipe Microreactor Power Conversion,” *Transactions. ANS Annual Meeting*, Indianapolis, IN, vol. 128, p. 998-991, (2023).
- [9] Chi, S. W., *Heat Pipe Theory and Practice: A Sourcebook*, Hemisphere Publishing Corporation, Washington, D. D., (1976).
- [10] Sternbentz, J. W., et al., “Special Purpose Nuclear Reactor (5 MW) for Reliable Power at Remote Sites Assessment Report,” INL/EXT-16-40741, INL, (2017).
- [11] Pidaparti, S. R., et al., “Technical and Economic Feasibility of Dry Air Cooling for the Supercritical CO₂ Brayton Cycle Using Existing Technology”, *Proc. sCO₂ Power Cycle Symposium*, (2016).